Journal of the Oman Medical Association

MDPI

Article

Systemic Explanation of *Alpinia officinarum*'s Analyzed Compounds and Its Anti-Cancer Mechanism Based on In Vitro Analysis and Network Pharmacology in Triple-Negative Breast Cancer

Shruti Sinnarkar [1], Poonam Suryawanshi [1], Amol Dilip Jadhav [2] and Vaibhav Sunil Ladke [3,*]

[1] Central Research Facility, Dr. D. Y. Patil Medical College, Hospital and Research Centre, Dr. D. Y. Patil Vidypeeth (Deemed to Be University), Sant Tukaram Nagar, Pimpri, Pune 411018, India; shrutisinnarkar25@gmail.com (S.S.); poonam.suryawanshi@dpu.edu.in (P.S.)
[2] Institute of Applied Biological Research and Development, Division of Nirav BioSolutions Pvt Ltd., Aundh, Pune 411067, India; amolraojadhav@gmail.com
[3] Integrative Health-From Discovery to Complete Care Consulting Oral & Maxillofacial Pathology, Kharadi, Pune 411014, India
* Correspondence: drvaibhavladke@gmail.com; Tel.: +91-9923132047

Abstract

Triple-negative breast cancer (TNBC) is an aggressive subtype of breast cancer lacking ER, PR, and HER2 expression, often associated with poor prognosis, early relapse, and resistance to conventional chemotherapy. Due to the limited availability of targeted therapies, natural products have gained attention for their structural diversity and potential anticancer activity. In this study, the methanolic extract of *Alpinia officinarum* (AO), a plant rich in bioactive compounds, was evaluated for its therapeutic potential in TNBC. The study combined in vitro experiments with in silico network pharmacology analysis. *Alpinia officinarum* exhibited notable cytotoxicity in MDA-MB-231 cells (IC_{50} = 31.1 µg/mL), inducing late-stage apoptosis, ROS reduction, mitochondrial depolarization, and upregulation of pro-apoptotic BAX gene. In silico analysis identified key hub genes—including AKT1, EGFR, and MAPK3—consistently enriched in cancer-related signalling pathways, with EGFR-TKI resistance pathway emerging as a principal axis of *Alpinia officinarum*'s anti-TNBC activity. Overall, the results suggest that *Alpinia officinarum* may serve as a promising multi-targeted therapeutic candidate for TNBC. By demonstrating both molecular and cellular mechanisms of action, these results lay the groundwork for the development of more effective and less toxic treatment strategies for TNBC.

Keywords: triple-negative breast cancer; *Alpinia officinarum*; in silico network pharmacology; in vitro; flow cytometry; apoptosis; MDA-MB-231; natural extract

Check for updates

Academic Editor: Rashid Al Abri

Received: 27 July 2026
Revised: 31 August 2026
Accepted: 24 September 2026
Published: 7 October 2026

Copyright: © 2026 by the authors. Published by MDPI on behalf of the Oman Medical Association. Licensee MDPI, Basel, Switzerland. This article is an open access article distributed under the terms and conditions of the Creative Commons Attribution (CC BY) license.

1. Introduction

Cancer arises when cells escape intrinsic regulatory controls and proliferate unchecked. Brown et al. describe it as "a disease of uncontrolled proliferation by transformed cells subject to evolution by natural selection," a description that reflects the capacity of tumours to adapt, metastasise, and accumulate genetic and epigenetic alterations [1]. Globally, cancer remains a leading cause of mortality, with more than 14 million new cases diagnosed each year; in India alone, incidence exceeds 1.1 million annually [2]. Major contributing lifestyle factors include physical inactivity, tobacco use, and poor dietary habits [3].

Preventive strategies are therefore receiving growing emphasis. One such approach is cancer chemoprevention, which involves the use of vaccines or pharmacological agents to inhibit, delay, or reverse carcinogenesis, thereby helping to reduce disease incidence [4]. Among women, breast cancer predominates, accounting for roughly one-quarter of female malignancies and 685,000 deaths worldwide in 2020 [5]. Risk rises with weight gain after adolescence, obesity, menopausal hormone therapy, alcohol intake, limited physical activity, and reproductive variables such as early menarche, late first pregnancy, and nulliparity, whereas breastfeeding confers protection [6].

Breast tumours are staged by tumour size, lymph-node status, metastatic spread, and biomarker expression—most notably oestrogen receptor (ER), progesterone receptor (PR), and ERBB2/HER2. Tumours lacking all three markers are classified as triple-negative (TNBC). TNBC represents 10–15% of breast cancers yet is highly invasive, genomically heterogeneous, and prone to relapse within five years, leading to a markedly poorer prognosis than non-TNBC disease [7,8]. Early-stage TNBC is managed surgically with adjuvant chemotherapy, whereas advanced stages require systemic regimens; however, the targeted therapies available for ER- or HER2-positive tumours are absent for TNBC [9,10]. Anthracycline- and taxane-based chemotherapy remains standard, but initial chemosensitivity is often followed by rapid resistance and recurrence—the so-called "triple-negative paradox". Given TNBC's aggressive biology, elevated EGFR expression, and pro-inflammatory milieu, new treatment avenues—among them bioactive natural compounds—are urgently needed to improve survival and reduce treatment-related morbidity [11].

While conventional chemotherapeutic agents are widely used in cancer treatment, their effectiveness is often limited by drug resistance, toxicity, and severe side effects. In recent years, natural products have emerged as promising alternatives due to their therapeutic potential and reduced toxicity. Nearly 80% of U.S. Food and Drug Administration (FDA)-approved anticancer drugs are derived from or inspired by natural sources, with plants, marine organisms, and fungi contributing a large share. Well-known examples such as Taxol and vinblastine demonstrate how structurally unique compounds, accessible only through natural isolation, can operate via novel mechanisms. In this light, *Alpinia officinarum*, with its diverse phytochemical profile, offers a compelling natural source of bioactive compounds that may help manage cancers, including breast cancer, while potentially minimizing the adverse effects associated with conventional chemotherapy [4,12].

Alpinia officinarum (AO), commonly known as lesser galangal, is a medicinal and culinary herb from the Zingiberaceae family. Native to southern China and widely cultivated in Southeast Asia, it grows up to 1–1.5 m tall and produces a dark brown, aromatic rhizome. Phytochemical investigations have catalogued more than 90 constituents from AO, dominated by phenolic compounds—particularly diarylheptanoids—alongside abundant flavonoids, volatile oils, glycosides, and sesquiterpenes. These metabolites underpin a broad pharmacological profile: traditional formulations employ AO to relieve pain, stimulate digestion, and aid flu symptoms, while contemporary studies attribute to its extracts pronounced antibacterial, gastroprotective, anti-inflammatory, analgesic, memory-enhancing, and notably anti-tumour activities. In light of the adverse effects associated with many synthetic or biologic therapeutics, the diverse bioactivities and long history of safe culinary use make AO an attractive source of natural lead compounds for cancer research [13,14].

Over the past decade, network pharmacology has reshaped drug discovery by shifting the focus from single targets to the dynamic, interconnected signalling networks that actually drive diseases such as cancer. By integrating computational biology with network analysis, this approach maps drug–target interactions across entire cellular systems, allowing researchers to identify synergistic target combinations, predict multi-target drug

effects, and design strategies to overcome resistance while minimizing toxicity [15,16]. Computational models and algorithms thus narrow the search for optimal multi-target agents, accelerating the discovery of effective treatments that engage the disease network at multiple nodes.

In this study, we employed a combination of in vitro and in silico approaches to investigate the anticancer potential of *Alpinia officinarum* (AO) in triple-negative breast cancer (TNBC). A series of cellular assays were performed on the highly aggressive MDA-MB-231 cell line to evaluate the cytotoxic, anti-migratory, apoptotic, and anti-oxidative effects of AO, thereby establishing its anti-cancer activity. To further support and correlate these experimental findings, in silico network pharmacology was employed to identify gene–target interactions and signalling pathways modulated by AO's bioactive compounds in TNBC. Together, these complementary strategies aim not only to confirm AO's therapeutic efficacy but also to clarify the molecular framework of its action, offering insights for future drug development. Similar integrated network-pharmacology/experimental-validation frameworks have recently been applied to other natural compounds in TNBC, e.g., nomilin [17], underscoring the value of this combined approach.

2. Materials and Methods

2.1. In Vitro Analysis of the Anticancer Activity of Alpinia officinarum Methanol Extract

2.1.1. Cell Culture and Maintenance

MDA-MB-231 (Triple-Negative Breast Cancer) cells were obtained from the National Centre for Cell Sciences (NCCS) in Pune. At 37 °C, these cells were grown in Minimal Essential Medium (MEM; Gibco) medium. The media was enriched with 10% Fetal Bovine Serum (FBS) and 1% antimycotic-antibiotic solution from GibcoTM. To promote cell growth and viability, the cells were kept in a humidified, 5% CO_2-enriched atmosphere at 37 °C.

2.1.2. Plant Material and Extraction of *Alpinia officinarum*

Dried rhizomes of *Alpinia officinarum* were purchased from the Kerala market and authenticated by the Department of Botany, Agharkar Research Institute, Pune (voucher specimen no. R-138). The rhizomes (250 g) were ground and extracted by maceration using methanol at room temperature (24 h × 3). The extract was filtered and concentrated on a rotary evaporator under reduced pressure at 40 °C to obtain 17.25 g of viscous extract (≈6.9% *w*/*w* yield). No chemical fingerprinting (e.g., HPLC, GC–MS or LC-MS/MS) of this batch was performed; compound identification in this study therefore relies on IMPPAT database-level annotation rather than experimentally confirmed composition of the extract used in this study.

2.1.3. Stock Solutions Preparation

For cytotoxicity assessment on MDA-MB-231 cells, *Alpinia officinarum* (AO) extract was first weighed at 10 mg and completely solubilised in 1 mL of dimethyl-sulfoxide (DMSO), generating a 10 mg/mL primary stock that was stored at room temperature. A 1 mg/mL working stock was produced by diluting the primary solution ten-fold in complete growth medium, followed by sterilization via filtration through a 0.22 µm membrane. Final dilutions of 5, 10, 20, 40, 60, and 80 µg/mL were prepared from this working stock in complete MEM media. Throughout all treatments, the DMSO content was maintained below 0.1% (*v*/*v*). Carboplatin, an established chemotherapeutic agent, was included as the positive control.

2.1.4. Cytotoxicity Assay of *Alpinia officinarum*

Cell cytotoxicity was evaluated using the MTT assay. MDA-MB-231 cells were seeded in 96-well plates at a density of 5×10^4 cells/mL. After adherence, cells were treated with varying concentrations of AO extract ranging from 5 to 80 µg/mL. Carboplatin, used as the reference drug, was applied in concentrations between 10 and 80 µg/mL. Post-treatment, 10 µL of MTT reagent (5 mg/mL) was added to each well and incubated for 4 h to allow for formazan formation. Subsequently, 100 µL of DMSO was added to solubilize the formazan crystals. Absorbance was measured at 570 nm using a Multiskan SkyHigh plate reader (Thermo Fisher Scientific, Waltham, MA, USA), reflecting the number of metabolically active cells. The IC_{50} values were calculated in Microsoft Excel and used for subsequent experiments.

2.1.5. Apoptosis Analysis

Apoptosis was evaluated using the FITC Annexin V/Dead Cell Apoptosis Kit (Invitrogen-Molecular Probes®, Eugene, OR, USA). Following a 24 h treatment period, MDA-MB-231 cells were rinsed with cold 1X phosphate-buffered saline (PBS). Untreated cells served as negative controls for the assay. The stained cells were then analyzed by flow cytometry, detecting fluorescence at emission wavelengths of 530 nm and above 575 nm [18].

2.1.6. Cell Cycle Analysis

After washing with 1X PBS and trypsinization, both untreated and treated MDA-MB-231 cells (with AO and Carboplatin) were collected 24 h post-treatment. The harvested cells were treated with a staining solution containing RNase A (25 µL of 20 mg/mL, Invitrogen), 2 mM $MgCl_2$ (Sigma), and propidium iodide (5–10 µL of 100 µg/mL, Invitrogen), for 10–15 min at room temperature. Subsequently, cell cycle analysis was performed using a BD Biosciences FACS machine San Jose, CA, USA.

2.1.7. Reactive Oxygen Species [ROS]

Reactive oxygen species (ROS) production was evaluated using flow cytometry with the fluorescent probe DCFH-DA [19]. MDA-MB-231 cells were seeded in 6-well plates and allowed to grow for 24 h until 70–80% confluency was achieved. Cells were then exposed to AO and Carboplatin treatment at their respective IC_{50} concentrations. (Extract stocks were prepared as detailed in Section 2.1.2.) Fluorescence measurements were conducted using a Beckman Coulter Cytomics FC 500 flow cytometer, with excitation and emission wavelengths set at 495 nm and 520 nm, respectively.

2.1.8. Mitochondrial Membrane Potential (ΔΨm)

Mitochondrial membrane potential (ΔΨm) in MDA-MB-231 cells was evaluated using the MitoProbe™ $DiIC_1(5)$ Assay Kit, following the manufacturer's protocol. The assay utilizes a cyanine-based dye, $DiIC_1(5)$, that selectively responds to changes in mitochondrial membrane potential, along with carbonyl cyanide m-chlorophenylhydrazone (CCCP), a known uncoupling agent that disrupts ΔΨm for experimental purposes. $DiIC_1(5)$ readily diffuses into the cytoplasm and accumulates within mitochondria exhibiting intact membrane potential, emitting strong far-red fluorescence, proportional to the ΔΨm.

2.1.9. Wound Scratch Assay

To examine the anti-migratory effect of *Alpinia officinarum* (AO), a wound healing assay was performed using MDA-MB-231 cells. After seeding the cells at a density of 2×10^5 cells/mL in 24-well plates and reaching over 90% confluency, a straight-line scratch was made at the center of each well using a sterile 200 µL pipette tip. Cells were washed

with 1X PBS, treated with AO or left untreated (control), and incubated in medium with 5% serum at 37 °C. Scratch images were documented at 0 and 24 h using a Magnus INVI phase-contrast microscope. The assay was performed in triplicate [20].

2.1.10. RNA Isolation and RT-PCR

Following treatment with the desired concentrations of test compounds, cultured cells were harvested for RNA isolation. Total RNA was then extracted using the TRIzol™ reagent (Invitrogen, Cat. No. 15596018) according to the manufacturer's protocol. The expression levels of key apoptosis- and proliferation-related genes—including BAD, BAX, BCL2, and c-MYC—were analyzed in this study. Primer sequences used for gene amplification are provided in Supplementary Table S1 [ST:1].

2.1.11. Statistical Analysis

All experiments were performed in triplicate, and results are expressed as mean ± standard deviation (SD). Statistical analysis was carried out using GraphPad Prism version 8. Two-way ANOVA followed by Tukey's multiple comparisons test was applied to assess significance between treatment groups and the control. Statistical significance for all comparisons was set at $p < 0.05$, and was further denoted as **** $p < 0.0001$, *** $p < 0.001$, and ** $p < 0.01$. Formal normality/variance-homogeneity testing was not performed given the small per-group replicate number ($n = 3$), and parametric ANOVA was used following standard practice for this assay type.

2.2. In Silico Analysis and Correlation of the Anticancer Effects of Alpinia officinarum

2.2.1. Identification of Bioactive Compounds in *Alpinia officinarum* Methanolic Extracts

The IMPPAT (Indian Medicinal Plants, Phytochemistry, and Therapeutics) database was utilized to identify bioactive compounds present in the *Alpinia officinarum* (AO) extract, including constituents from both the root and rhizome. A total of 66 bioactive compounds were identified. The names of the phytochemicals were documented and cross-referenced with their corresponding Compound IDs on the PubChem database. Simplified Molecular Input Line Entry System (SMILES) notations were also retrieved for each compound where available to facilitate downstream target identification and computational analysis. The identified compounds were further evaluated according to Lipinski's Rule of Five [21], considering molecular weight, lipophilicity (XLogP), hydrogen-bond donor count, and hydrogen-bond acceptor count as criteria for drug-likeness. Of the 66 compounds, 59 had PubChem structures/SMILES available and satisfied the applied drug-likeness criteria, and were therefore selected for further analysis.

2.2.2. Target Gene Identification of AO-Derived Bioactive Compounds

To predict the potential gene targets of all identified bioactive compounds (BAs), the SwissTargetPrediction database (http://www.swisstargetprediction.ch/ accessed on 26 July 2026) [22] was employed. This tool was used to determine the most likely protein targets associated with each compound based on their chemical structure.

2.2.3. Target Genes Associated with Triple-Negative Breast Cancer

The DisGeNET platform (v7.0; http://www.disgenet.org/ accessed on 26 July 2026) was employed to retrieve disease-associated gene targets. DisGeNET is a comprehensive database that integrates extensive information on genes and variants linked to various human diseases. Genes implicated in triple-negative breast cancer (TNBC) were extracted from the database and subsequently compared against the predicted targets of each bioactive compound identified in *Alpinia officinarum* (AO). Overlapping genes common to both datasets were identified and selected for further investigation.

2.2.4. PPI Network of Common Genes and Identification of Hub Genes

Protein–protein interactions (PPIs) play a vital role in cellular processes and are essential for understanding complex biological systems. To explore the PPI network of genes common to targets of AO-derived BA and TNBC-associated genes, the overlapping gene set was analyzed using the STRING database (version 11.5; http://string-db.org/ accessed on 26 July 2026) [23] with "Homo sapiens" as the selected species and a high-confidence interaction score threshold of >0.9. The resulting network was visualized and further analyzed using Cytoscape (version 3.10.1; https://cytoscape.org/), a widely adopted bioinformatics tool for data integration and visualization [24]. To detect highly interconnected clusters and prioritize key proteins, the cytoHubba plugin (version 0.1) was utilized, identifying key hub genes based on the highest degree values within the PPI network.

2.2.5. Pathway Enrichment Analysis of Common Genes

Gene Ontology (GO) and KEGG (Kyoto Encyclopedia of Genes and Genomes) pathway enrichment analyses of the common genes were conducted using the Database for Annotation, Visualization, and Integrated Discovery (DAVID, version 6.8). DAVID enables systematic functional annotation of gene lists, while KEGG provides comprehensive, graphically mapped biochemical pathways relevant to cellular and disease processes [25]. GO offers a hierarchical framework for classifying gene functions in terms of biological processes, molecular functions, and cellular components [26]. Based on clinical and pathological relevance, breast-cancer-associated pathways were prioritized from the enriched results. Data visualization was performed using the Bioinformatics cloud platform (http://www.bioinformatics.com.cn/ accessed on 26 July 2026), a specialized tool for online data analysis and presentation. To visualise and interpret the enriched gene sets, the key pathways and genes were further visualized using ShinyGO, an interactive graphical tool [27].

2.2.6. Expression Analysis of Hub Genes

To evaluate the clinical relevance of the identified hub genes, gene expression and survival analyses were performed using the UALCAN portal (https://ualcan.path.uab.edu/) [28], an interactive cancer data analysis platform developed by the University of Alabama at Birmingham. UALCAN facilitates in silico validation of genes by enabling researchers to explore transcriptomic and proteomic profiles across various cancer types. It utilizes TCGA (The Cancer Genome Atlas) data to provide comparative plots that simplify data analysis and interpretation. The top 10 hub genes identified through Cytoscape analysis were further assessed using UALCAN to determine their differential expression in breast cancer, stage-wise expression patterns, and association with patient prognosis.

2.2.7. Immune Infiltration Analysis

The Tumour Immune Estimation Resource version 2.0 (TIMER2.0) web server (http://timer.cistrome.org/ accessed on 26 July 2026) was used to link the selected hub genes (AKT1, STAT3, TNF, HIF1A, EGFR, ALB, SRC, HSP90AA1, ESR1, and MAPK3) and immune cell infiltration in Breast Invasive Carcinoma (TIMER2.0 uses gene expression profiles to infer the abundance of tumor-infiltrating immune cells across The Cancer Genome Atlas (TCGA) datasets). We examined the correlation between gene expression levels and infiltration of B cells, $CD8^+$ T cells, $CD4^+$ T cells, macrophages, neutrophils, and dendritic cells in the TCGA-BRCA cohort with the Gene module of TIMER2.0. Gene expression levels were normalised to log 2 Transcripts Per Million (TPM). Partial Spearman's correlation analysis corrected for tumour purity reduced the confounding effects of tumour cellularity. The partial correlation

coefficient (partial cor) indicated the strength and the direction of the association, and the statistical significance was determined by the TIMER2.0 *p*-value. Positive correlation coefficients indicated gene expression promoting immune cell infiltration, while negative values indicated the opposite. Correlations between hub gene expression and immune infiltration were shown by scatter plots from TIMER2.0. Each plot shows the tumour samples, locally fitted regression curve, partial correlation coefficient and *p*-value. Statistical significance was set at $p < 0.05$.

3. Results

3.1. In Vitro Analysis of the Anticancer Activity of Alpinia officinarum Methanol Extract on MDA-MB-231 Cell Line

3.1.1. Cytotoxicity of AO Against MDA-MB-231 Cells

Treatment with varying concentrations of *Alpinia officinarum* (AO) (5, 10, 20, 40, 60, and 80 µg/mL) and Carboplatin (10, 20, 40, and 80 µg/mL) exhibited a strong, dose-dependent cytotoxic effect on MDA-MB-231 cells. The IC_{50} value for AO was determined to be 31.1 ± 4.5 µg/mL, while Carboplatin showed an IC_{50} of 31.6 ± 8.1 µg/mL. Based on these findings, the IC_{50} concentration of AO (31.1 ± 4.5 µg/mL) was selected for all subsequent experiments.

3.1.2. Impact of AO on Proliferation and Cell Cycle in MDA-MB-231 Cells

To further investigate the anticancer effects of AO, MDA-MB-231 cells were treated with the IC50 concentration of AO for 24 h and analysed for proliferation and cell cycle distribution using flow cytometry. In untreated control cells, a typical cell cycle profile was observed, with distinct phases: G0/G1 (64.5 ± 2.05%), S (9.25 ± 0.24%), and G2/M (22 ± 1.13%). However, AO treatment induced a significant shift in cell cycle distribution. Specifically, there was a marked decrease in the G0/G1 (39.4 ± 0.07%) and G2/M (9.78 ± 1.15%) populations, alongside a substantial increase in the sub-G1 population (43.1 ± 0.84%), which is mostly associated with apoptotic and dead cells (Figure 1A,B).

3.1.3. Effect of AO on Apoptosis in MDA-MB-231 Cells

Next, we examined the effect of AO on apoptosis in MDA-MB-231 cells. In the control group, the majority of cells were live (93.5 ± 2.9%), with a small fraction in the early apoptotic phase (3.28 ± 0.79%) and very few in the late apoptotic or necrotic phase (1.96 ± 1.4%). However, following AO treatment, a pronounced shift was observed. The percentage of live cells decreased substantially to 51.6 ± 3.8%, while the early and late apoptotic populations increased significantly to 7.12 ± 3.3% and 23.5 ± 1.4%, respectively. These findings indicate that AO treatment at its IC50 concentration effectively induces apoptosis (Figure 1C,D).

3.1.4. Impact of AO on Intracellular ROS Measurement and Mitochondrial Membrane Potential (ΔΨm) in MDA-MB-231 Cells

Next, we assessed the effect of AO on intracellular ROS levels and mitochondrial membrane potential in MDA-MB-231 cells. Figure 2A presents representative plots illustrating intracellular ROS levels before and after AO treatment, while Figure 2C displays the corresponding plots for mitochondrial membrane potential in MDA-MB-231 cells.

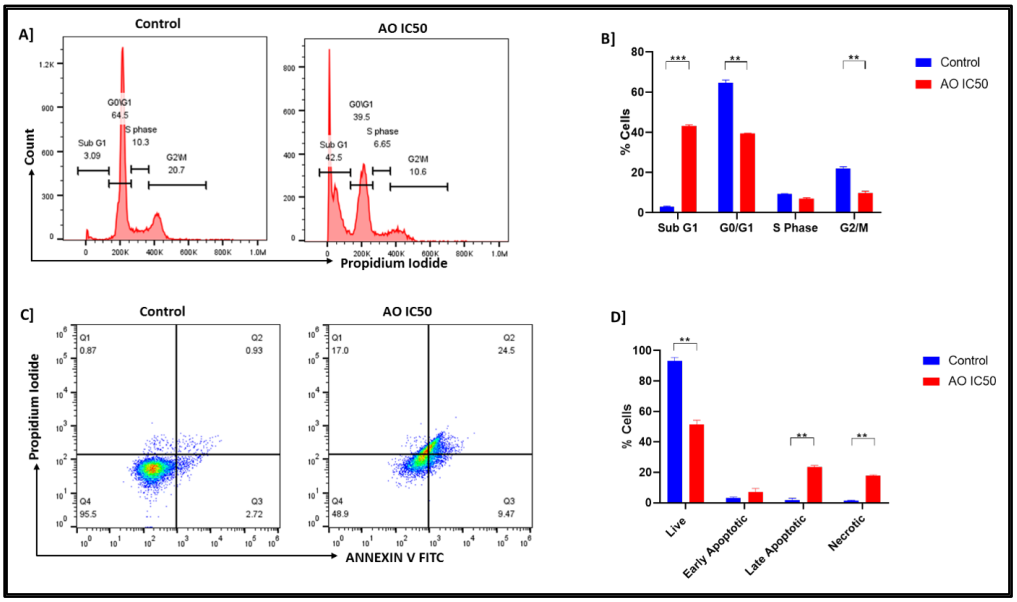

Figure 1. Effect of AO treatment on cell cycle and apoptosis in *MDA MB231* cells. (**A**) Histogram represents different stages of cell cycle in *MDA-MB-231* cells in control (left) and after treatment of AO (right) for 24 h using Propidium iodide. (**B**) Bar graph shows the percentages of live, early apoptotic, late apoptotic and necrotic cells in control (blue) and after treatment of AO (red) for 24 h. Error bar shows mean with standard deviation. ** $p < 0.01$, *** $p < 0.001$. (**C**) Dot plot shows apoptosis ratios of *MDA-MB-231* cells in control (left) and after treatment of AO (right) for 24 h. using Propidium iodide and Annexin-V FITC. (**D**) Bar graph shows the percentages of cells in sub *G1*, *G0/G1*, *S* and *G2/M* phases in control (blue) and after treatment of AO (red) for 24 h.

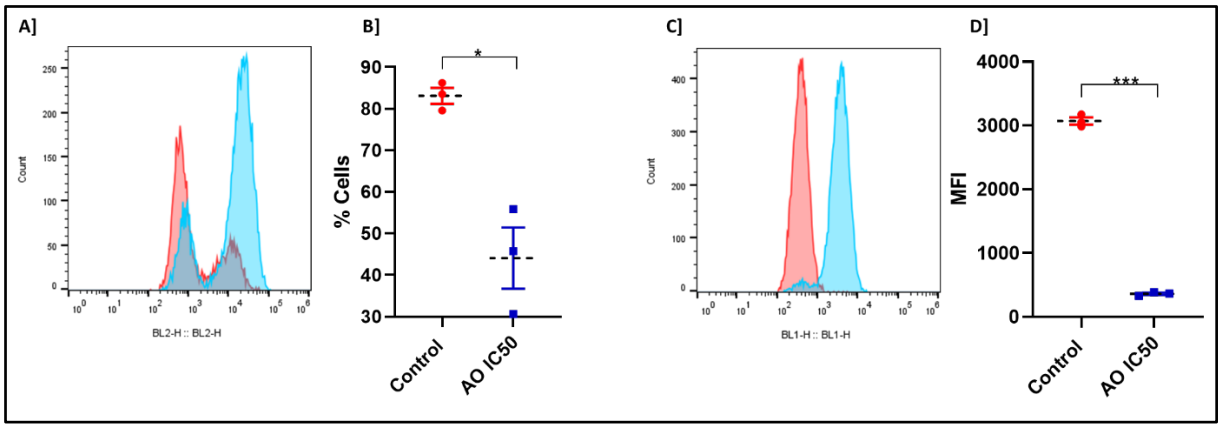

Figure 2. Impact of AO treatment on ROS generation and membrane mitochondrial potential in MDA-MB-231 cells (**A**). The histogram shows the extent of reactive oxygen species (ROS) generation before (blue) and after the treatment of AO (red) in MDA-MB-231 cells. (**B**) The scatter dot plot shows the quantitative analysis of ROS generation before (red) and after (blue) the treatment of AO in MDA-MB-231 cells. (**C**) The histogram showing the extent membrane mitochondrial potential ($\Delta\Psi m$) before (blue) and after the treatment of AO (red) in MDA-MB-231 cells. (**D**) The scatter dot plot shows the quantitative analysis of membrane mitochondrial potential before (red) and after (blue) the treatment of AO in MDA-MB-231 cells. Error bar shows mean with standard deviation. * $p < 0.05$, *** $p < 0.001$.

AO treatment resulted in a significant decrease in ROS levels (44.07 ± 12.73%) compared to the control (83.10 ± 3.31%) (Figure 2B). Moreover, AO treatment led to a dramatically reduced mitochondrial membrane potential (Mean Fluorescence Intensity, MFI:

360 ± 29.46) compared to the control (MFI: 3071 ± 96.46) (Figure 2D) suggesting mitochondrial depolarization and potential dysfunction.

3.1.5. AO Treatment Modulates Expression of BCL-2 Family Proteins in MDA-MB-231 Cells

Figure 3 illustrates the fold change in gene expression of four key proteins in the BCL-2 family (BAD, BAX, BCL-2, and cMYC) in response to AO treatment compared to a control. Overall, the figure shows that AO treatment significantly increases the expression of BAX, while slight decreasing the expression of BAD. On the other hand, AO treatment shows little effect on BCL-2 and cMYC gene expression.

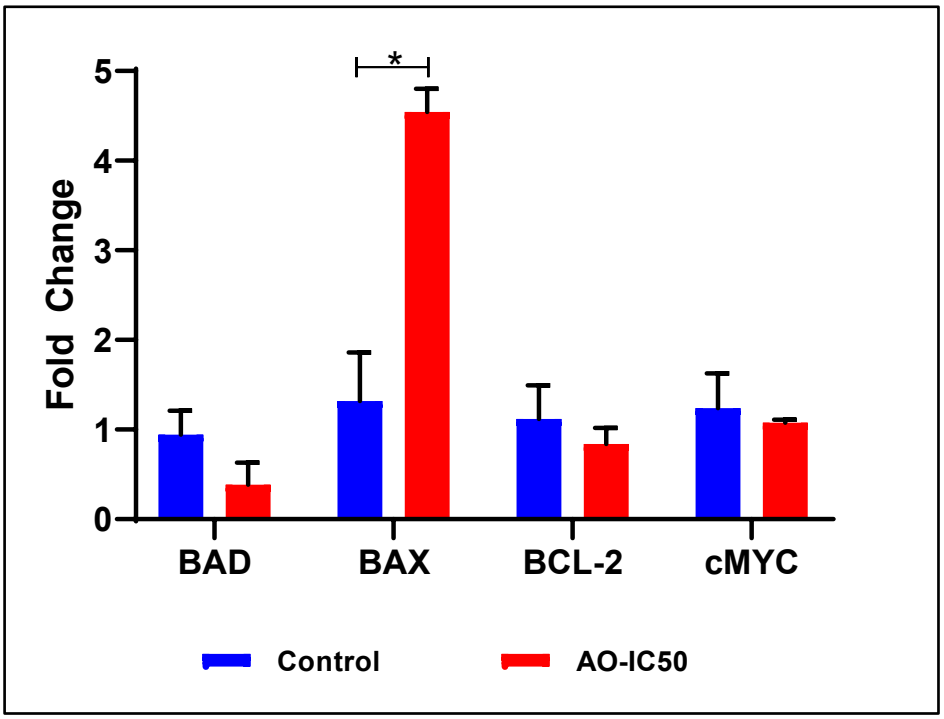

Figure 3. Effect of AO treatment on different genes expression involved in apoptosis. The bar graph shows fold change in the gene expression levels of BAD, BAX, BCL-2 and cMYC, before (Blue) and after (red) the treatment of AO in MDA-MB-231 cells. Error bar shows mean with standard deviation. * $p < 0.05$.

This result suggests that AO promotes apoptosis, via regulating the expression of critical BCL-2 proteins. The large increase in BAX, a potent pro-apoptotic factor, is a notable finding that suggests a possible mode of action for AO.

3.1.6. Anti-Migratory Effect of AO on MDA-MB-231 Cells

Cells treated with AO at the IC_{50} concentration showed strong inhibition of migration after 24 h, while those treated with IC_{25} exhibited limited migration, indicating partial inhibition. In contrast, the control group showed substantial wound closure due to active proliferation and migration (Figure 4).

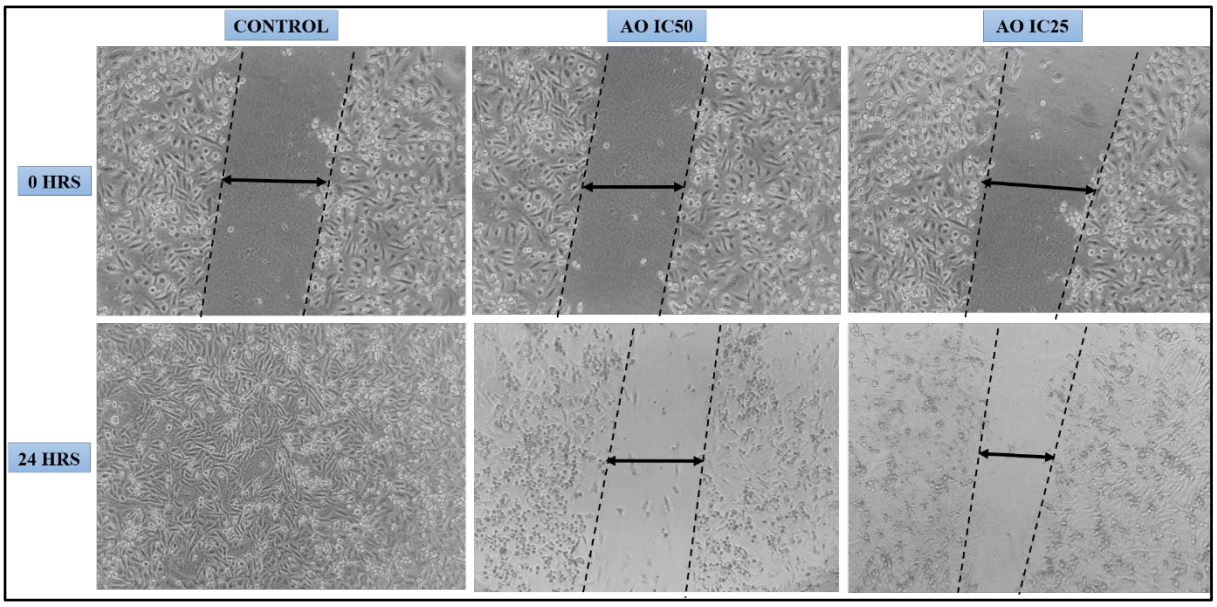

Figure 4. Wound scratch assay results. MDA-MB-231 cells treated with AO (IC_{50}: 31.1 µg/mL) for 24 h showed reduced migration in the scratch assay, visualized at 0 and 24 h (100× magnification). Control and treated groups are shown in the first and second panels, respectively.

3.2. In Silico Analysis of Alpinia officinarum and Triple Negative Breast Cancer (TNBC)

3.2.1. Potential Bioactive Compounds of AO and TNBC-Associated Genes

A total of 66 bioactive compounds (BA) present in *Alpinia officinarum* (AO) extract were retrieved from the IMPPAT (Indian Medicinal Plants, Phytochemistry and Therapeutics) database. Of these, 59 compounds had corresponding structures/SMILES available in the PubChem database and satisfied the applied Lipinski's Rule of Five criteria, and were therefore considered for subsequent computational analysis. To identify genes associated with triple-negative breast cancer (TNBC), the DisGeNET database was queried using the term "Triple-negative breast cancer," which yielded 1674 relevant gene targets. For target prediction of the 59 compounds, the SwissTargetPrediction database was employed, and predicted targets were obtained only for 56 compounds where 3 compounds did not show any targets, resulting in 689 unique predicted targets after removal of duplicates.

3.2.2. Common Genes Between TNBC and Bioactive Compounds of AO

By comparing the 689 genes associated with bioactive compounds (BA) of AO to the 1674 genes linked to triple-negative breast cancer (TNBC), a total of 199 overlapping genes were identified. This shared gene set is illustrated in Figure 5.

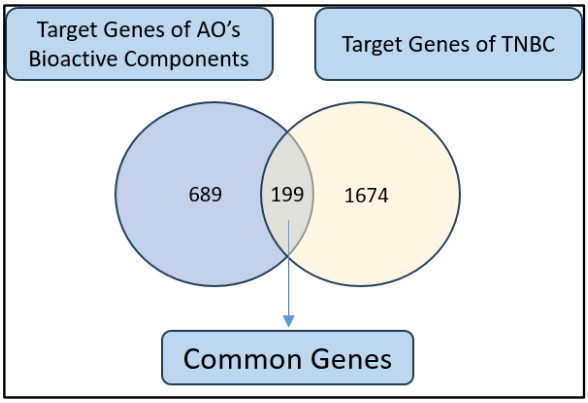

Figure 5. Common genes between AO and TNBC.

3.2.3. Identification of Hub Genes

The STRING database was utilized to analyze protein–protein interactions (PPIs) among the 199 common genes identified. This PPI network was further examined using Cytoscape 3.10.1 to pinpoint hub genes. The network exhibited a highly significant enrichment of interactions (p-value < 1.0×10^{-16}), suggesting that these proteins interact more extensively than expected compared to a random group of proteins with similar size and connectivity. By applying multiple algorithms within the cytoHubba plugin in Cytoscape, the top 10 hub genes were identified: AKT1, STAT3, TNF, HIF1A, EGFR, ALB, SRC, HSP90AA1, ESR1, and MAPK3, with AKT1 being the most prominent (Table 1, Figure 6).

Table 1. Identification of Hub Genes using different algorithms on CytoHubba.

Algorithms	MCC	MNC	Degree
Genes	STAT3	AKT1	AKT1
	HIF1A	STAT3	STAT3
	TNF	TNF	TNF
	MMP9	HIF1A	HIF1A
	AKT1	EGFR	EGFR
	ESR1	ALB	ALB
	SRC	HSP90AA1	SRC
	MTOR	SRC	HSP90AA1
	HSP90AA1	ESR1	ESR1
	MMP2	MAPK3	MAPK3

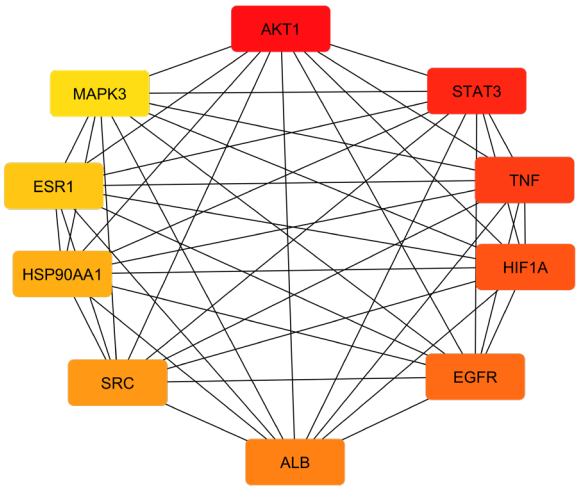

Figure 6. Top 10 Hub Genes of AO against TNBC.

The top 10 bioactive compounds of *Alpinia officinarum* (AO) were selected based on the number of hub genes they targeted in TNBC. These compounds were used to construct a compound–target network in Cytoscape, illustrating the interconnected gene targets of each compound (Figure 7A). To refine this network and highlight only the most highly connected genes, a degree-sorted subnetwork was generated, with CYP19A1 emerging as the highest-degree node, followed by others arranged in decreasing order counter-clockwise (Figure 7B).

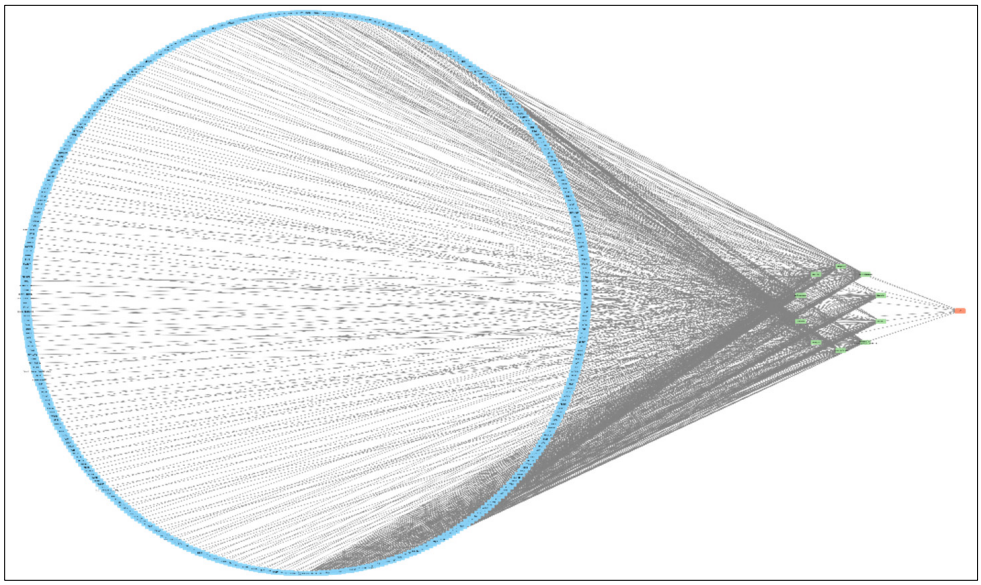

(**A**)

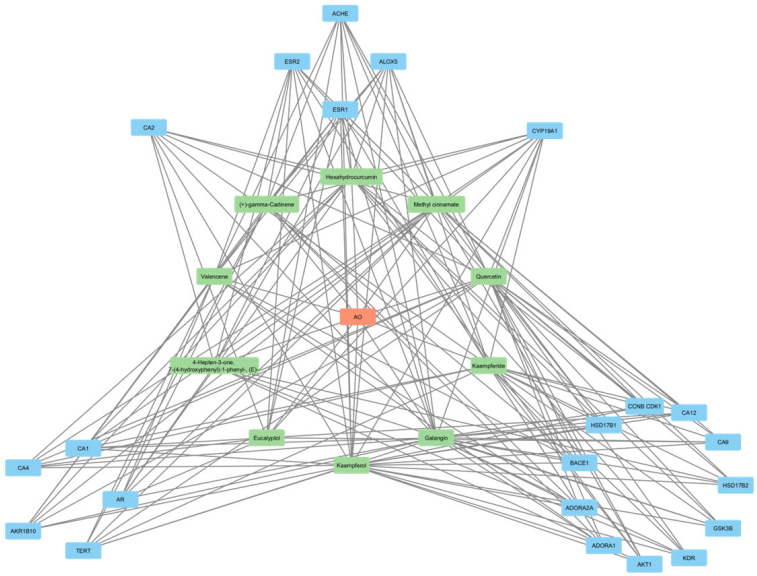

(**B**)

Figure 7. (**A**) Network of top 10 core bioactive compounds (green) of AO (orange) and their targets (blue) in TNBC. (**B**) Core bioactive compounds (green) of *Alpinia officinarum* (AO, orange) and their highly interconnected gene targets (blue) in TNBC. The target genes are degree-sorted, with CYP19A1 as the highest-degree node; others are arranged in decreasing order, counter-clockwise.

3.2.4. GO and KEGG Enrichment Analysis

Gene Ontology (GO) enrichment analysis of the 199 overlapping genes yielded approximately 35 enriched GO terms. Within the biological process (BP) category, the genes were primarily associated with transcriptional regulation, cell cycle control, apoptosis, mitosis, inflammatory response, and angiogenesis. The cellular component (CC) analysis revealed enrichment in structures such as the cytoplasm, plasma membrane, nucleus, extracellular matrix, and chromosome. In terms of molecular function (MF), the genes were predominantly involved in the activity of kinases, receptors, transferases, and chromatin regulators. The top 10 GO terms from each category are illustrated in Figure 8.

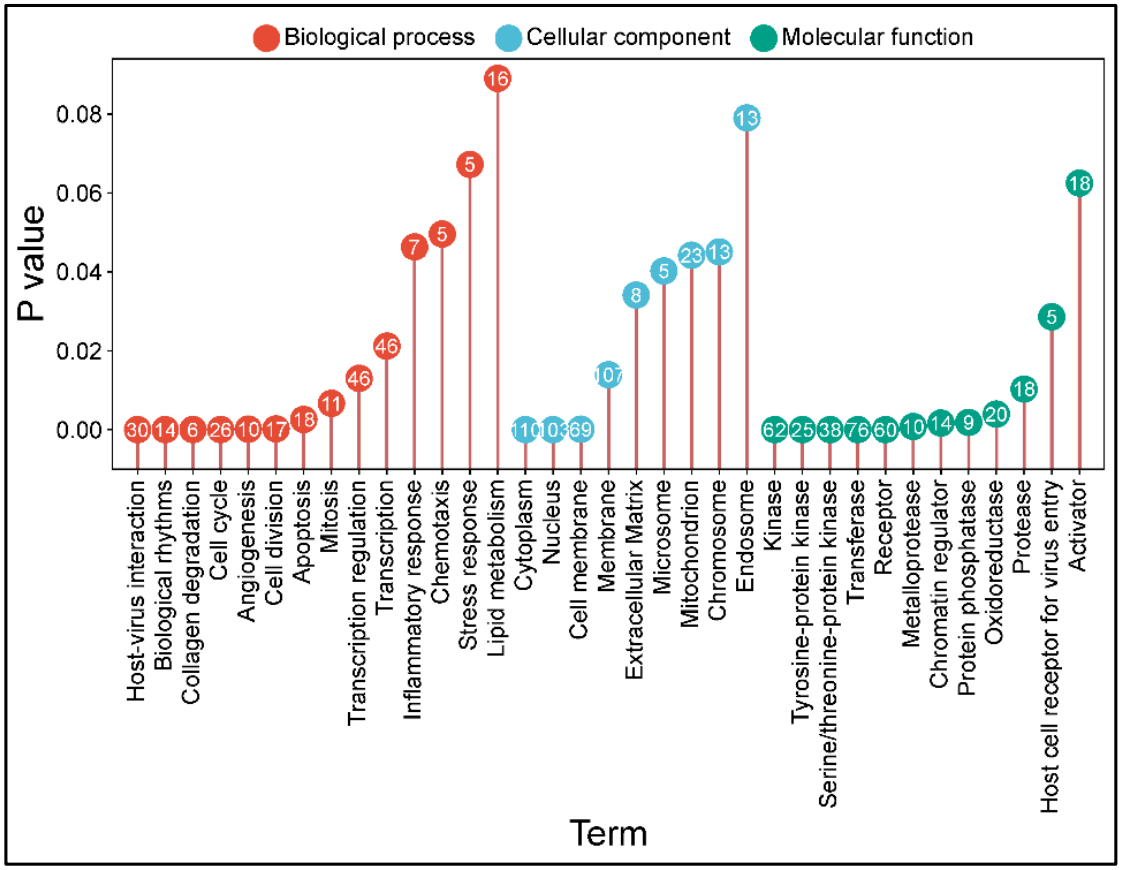

Figure 8. Top 10 biological processes (BP), cellular components (CC), and molecular functions (MF) obtained after GO enrichment analysis using DAVID Database for the common targets of AO and TNBC.

KEGG pathway enrichment analysis identified a total of 160 pathways associated with the 199 common genes. From these, the top 10 most significantly enriched pathways were selected for further investigation. Notably, the top 10 hub genes were found to be closely linked to several key cancer-related pathways, including the PI3K-Akt signalling pathway, apoptosis, proteoglycans in cancer, EGFR tyrosine kinase inhibitor resistance, microRNAs in cancer, pathways in cancer, and MAPK signalling pathway (Figure 9).

Across the ten most enriched KEGG pathways, five hub genes—MAPK3, AKT1, EGFR, STAT3, and SRC—were repeatedly identified. They showed a strong association with the EGFR tyrosine-kinase inhibitor (TKI) resistance pathway, a signalling cascade essential for cellular homeostasis. Mutations that confer TKI resistance can drive carcinogenesis by up-regulating EGFR, thereby enhancing key cellular processes such as proliferation, survival, angiogenesis, differentiation, and motility [29]. Overall (Table 2), these findings suggest that AO could mediate anticancer effects in breast cancer largely by modulating the EGFR-TKI resistance pathway, with apoptosis emerging as the principal downstream mechanism. The pathway map was further visualized and analyzed using ShinyGO [25,27,30], highlighting key gene interactions within this signalling network (Figure 10).

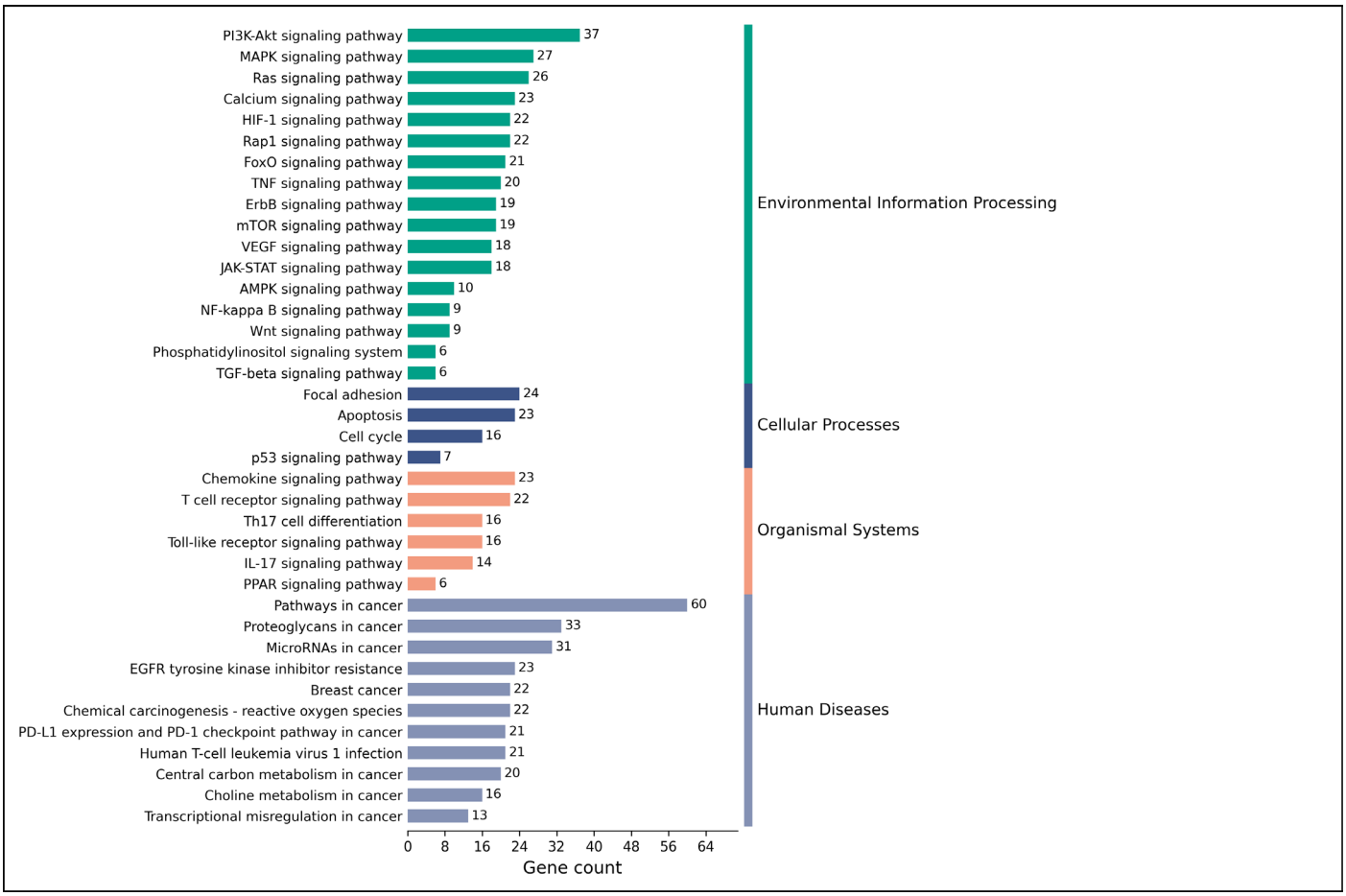

Figure 9. Top 38 pathways associated with common genes of AO and Breast Cancer. The X-axis states the Gene Count, while the Y-axis states the different pathways. The plot is further color-coded according to their categories.

Table 2. Top 10 pathways involving the common genes.

Term	Count	*p* Value	Fold Enrichment	Genes
hsa05200:Pathways in cancer	60	1.65×10^{-27}	5.221062077	RET, GSK3B, CXCL8, PIK3CD, PIK3CB, GLI1, IGF1R, PIM1, AKT1, PIM2, JAK2, JAK1, MAP2K1, HSP90AA1, CHUK, PRKCB, MMP1, DAPK2, MMP2, PRKCA, MMP9, RHOA, AR, PIK3CA, KIT, RARA, RARB, PPARG, RAF1, IL6ST, MET, EPAS1, HDAC1, PIK3R1, PTGS2, RASGRP1, HIF1A, EGFR, MAPK9, MAPK8, RXRA, ERBB2, MAPK1, VHL, MAPK3, NTRK1, NQO1, CREBBP, NOS2, WNT3A, STAT3, ESR1, MTOR, ESR2, PTK2, CDK6, CDK4, CDK2, MDM2, FGFR1
hsa04151:PI3K-Akt signaling pathway	37	4.74×10^{-15}	4.740541677	RET, GSK3B, FLT1, PIK3CD, PIK3CB, PIK3R1, EGFR, PIK3CG, IGF1R, RXRA, ERBB2, KDR, AKT1, MAPK1, JAK2, JAK1, MCL1, MAPK3, NTRK1, MAP2K1, HSP90AA1, SYK, CHUK, NOS3, PRKCA, MTOR, PTK2, NR4A1, CDK6, PIK3CA, CDK4, KIT, CDK2, MDM2, RAF1, MET, FGFR1

Table 2. *Cont.*

Term	Count	*p* Value	Fold Enrichment	Genes
hsa05205:Proteoglycans in cancer	33	2.49×10^{-19}	7.502717391	SRC, PIK3CD, PIK3CB, PIK3R1, HIF1A, TNF, EGFR, IGF1R, CTSL, ERBB2, KDR, AKT1, MAPK1, MAPK3, MAP2K1, PRKCB, WNT3A, MMP2, STAT3, PRKCA, PTPN11, MAPK14, MMP9, ESR1, RHOA, MTOR, PTK2, PIK3CA, MDM2, PTPN6, RAF1, MET, FGFR1
hsa05206:MicroRNAs in cancer	31	2.91×10^{-12}	4.60831243	ABCB1, HDAC1, PIK3CD, PIK3CB, PIK3R1, PTGS2, EGFR, ERBB2, PIM1, MAPK1, MCL1, MAPK3, ABCC1, MAP2K1, CREBBP, PRKCB, WNT3A, STAT3, PRKCA, MMP9, RHOA, MTOR, CDC25B, CYP24A1, CDK6, PIK3CA, MDM2, MDM4, RAF1, MET, EZH2
hsa04010:MAPK signaling pathway	27	9.48×10^{-10}	4.17423913	RET, FLT1, RASGRP1, TNF, EGFR, IGF1R, MAPK9, RPS6KA3, MAPK8, ERBB2, KDR, AKT1, MAPK1, MAPK3, NTRK1, MAP2K1, CHUK, PRKCB, PRKCA, MAPK14, CDC25B, NR4A1, KIT, PTPN7, RAF1, MET, FGFR1
hsa04014:Ras signaling pathway	26	3.36×10^{-11}	5.066770186	FLT1, PIK3CD, PIK3CB, PIK3R1, RASGRP1, EGFR, IGF1R, MAPK9, MAPK8, HTR7, KDR, AKT1, MAPK1, MAPK3, NTRK1, MAP2K1, CHUK, PRKCB, PRKCA, PTPN11, RHOA, PIK3CA, KIT, RAF1, MET, FGFR1
hsa04510:Focal adhesion	24	4.71×10^{-11}	5.483401157	GSK3B, MAP2K1, FLT1, PRKCB, SRC, PIK3CD, PRKCA, PIK3CB, PIK3R1, RHOA, EGFR, PTK2, IGF1R, MYLK, MAPK9, MAPK8, PIK3CA, ERBB2, KDR, AKT1, MAPK1, RAF1, MET, MAPK3
hsa01521:EGFR tyrosine kinase inhibitor resistance	23	4.78×10^{-19}	13.334375	GSK3B, MAP2K1, PRKCB, SRC, STAT3, PIK3CD, PRKCA, PIK3CB, PIK3R1, EGFR, MTOR, IGF1R, PIK3CA, AXL, ERBB2, KDR, AKT1, MAPK1, JAK2, RAF1, MET, JAK1, MAPK3
hsa04210:Apoptosis	23	8.49×10^{-14}	7.84375	NTRK1, MAP2K1, PARP1, CHUK, EIF2AK3, PIK3CD, PIK3CB, PIK3R1, TNF, CTSS, ERN1, MAPK9, MAPK8, PIK3CA, CTSL, AKT1, MAPK1, CAPN1, RAF1, CTSD, CTSB, MCL1, MAPK3
hsa04062:Chemokine signaling pathway	23	1.14×10^{-10}	5.527202073	GSK3B, ITK, MAP2K1, CXCL8, CHUK, PRKCB, SRC, STAT3, PIK3CD, PIK3CB, PIK3R1, RHOA, PIK3CG, PTK2, PIK3CA, CXCR2, PTK2B, AKT1, MAPK1, JAK2, RAF1, CCR5, MAPK3

3.2.5. External Validation of Hub Genes

To examine the varied expression of hub genes within breast cancer tissues and normal tissues, we utilized the UALCAN database. Our analysis revealed that AKT1, ESR1, and SRC mRNA levels were significantly elevated in breast cancer specimens compared to normal samples ($p < 0.01$) (Figure 11A).

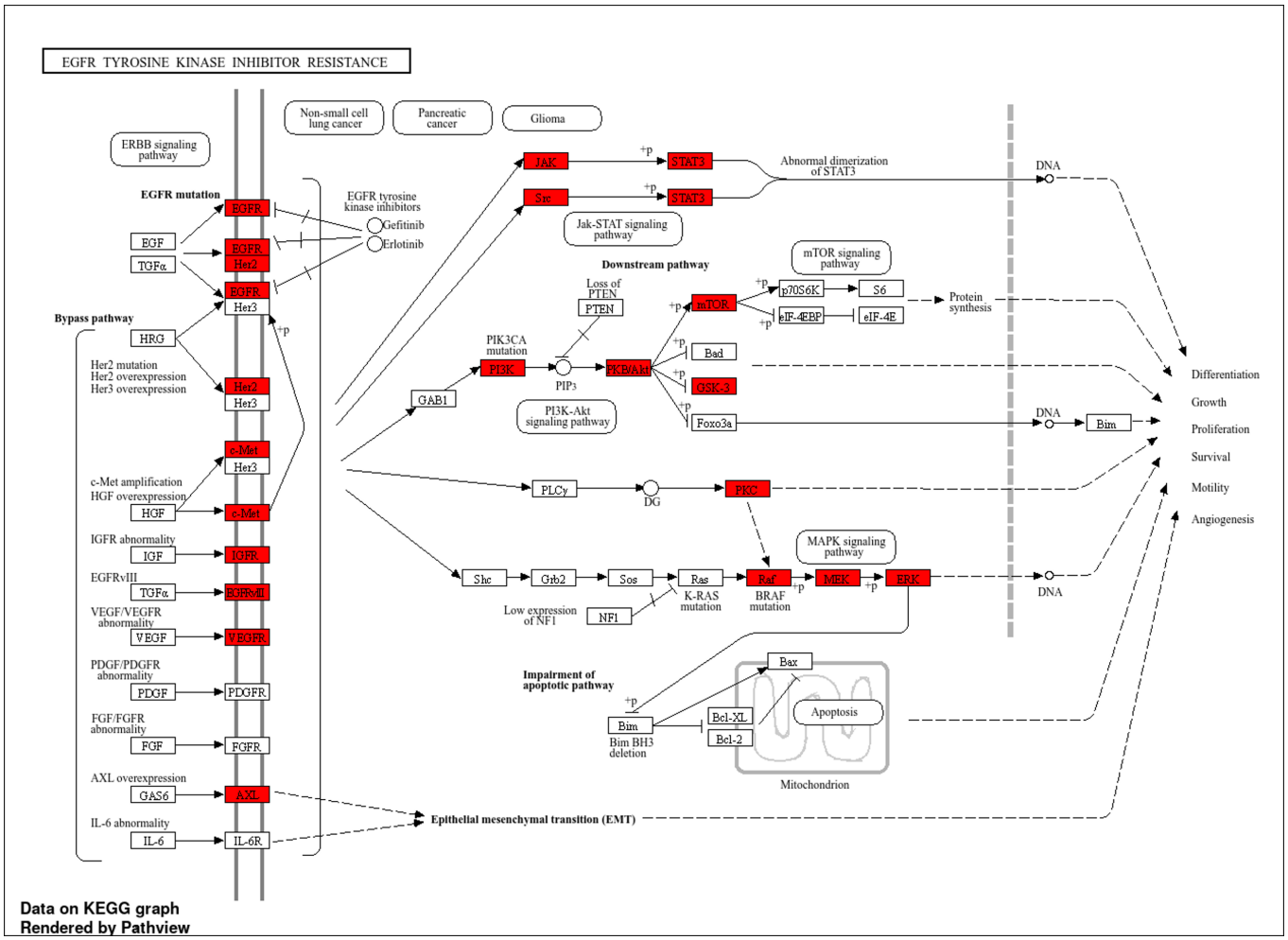

Figure 10. The EGFR tyrosine kinase inhibitor (TKI) resistance pathway map (ShinyGO), highlighting multiple common genes (in red) shared between AO and TNBC. The pathway connects with several others—such as apoptosis, PI3K-Akt, ERBB, mTOR, and JAK-STAT—leading to key cellular processes like growth, survival, proliferation, and angiogenesis.

Furthermore, we investigated the relationship between mRNA levels of the hub genes and the pathological stages of breast cancer. Stage-wise analysis showed that some oncogenic genes (AKT1, SRC, HSP90AA1 and ESR1) are upregulated throughout breast cancer progression whereas EGFR is downregulated in tumours compared to normal tissues. Most genes do not exhibit a clear stage-dependent up- or down-regulation, suggesting that their dysregulation is early rather than gradual during disease progression. The wide range of variation within each stage is indicative of the molecular heterogeneity of breast cancer (Figure 11B).

Among the ten hub genes analysed, only HSP90AA1 was significantly associated with overall survival ($p = 0.0026$). The other genes were not statistically significant for patient survival ($p > 0.05$), but several showed trends that might be interesting to explore further (Figure 11C).

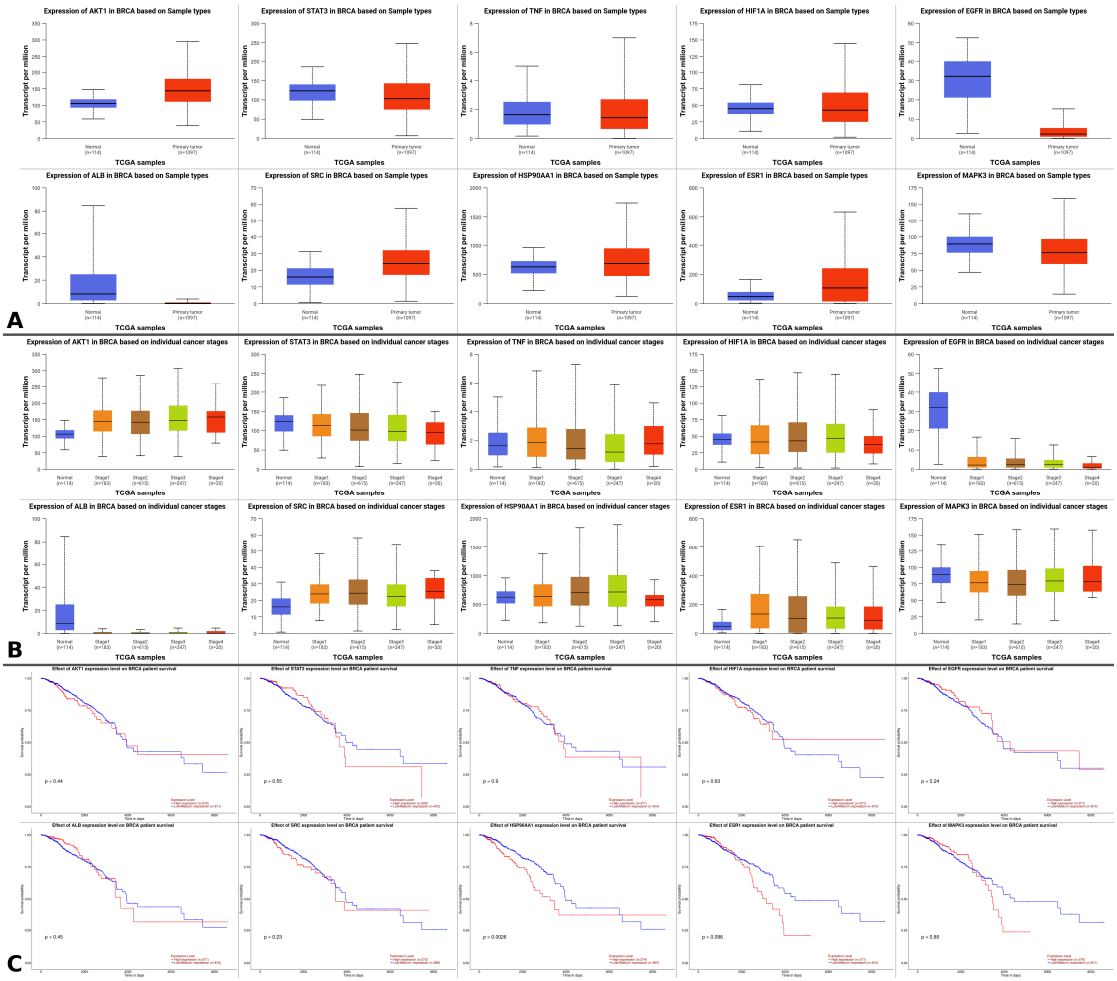

Figure 11. The mRNA expression levels of hub genes in The Cancer Genome Atlas (TCGA) database and the overall survival analyses of breast cancer patients. (**A**) mRNA expression levels in the UALCAN database [Boxplot of hub genes]. Red depicts Breast Cancer tissue, and blue depicts normal breast tissue. (**B**) mRNA expression levels in different pathological stages in the UALCAN database [Stage plot of hub genes]. (**C**) Survival analysis.

3.2.6. Immune Infiltration Analysis Using TIMER 2.0

TIMER immune infiltration analysis revealed distinct associations between hub gene expression and immune cell abundance in TCGA-BRCA. STAT3, TNF, HIF1A and EGFR were positively correlated with multiple immune cell populations (including $CD8^+$ T cells, $CD4^+$ T cells, macrophages, neutrophils and dendritic cells) and participated in the regulation of breast cancer immune microenvironment. In contrast, AKT1, SRC, HSP90AA1 and MAPK3 were weakly correlated with immune infiltration, suggesting these genes mainly regulate tumour intrinsic signalling pathways. ESR1 was negatively correlated with most immune cell populations and positively associated with tumour purity, which was consistent with the immune-cold phenotype of oestrogen receptor-positive breast cancers. Collectively, these results suggest that inflammatory and hypoxia-related genes are more tightly associated with immune cell recruitment, while genes involved in oncogenic signalling mainly influence tumour cell proliferation and survival (Figure 12).

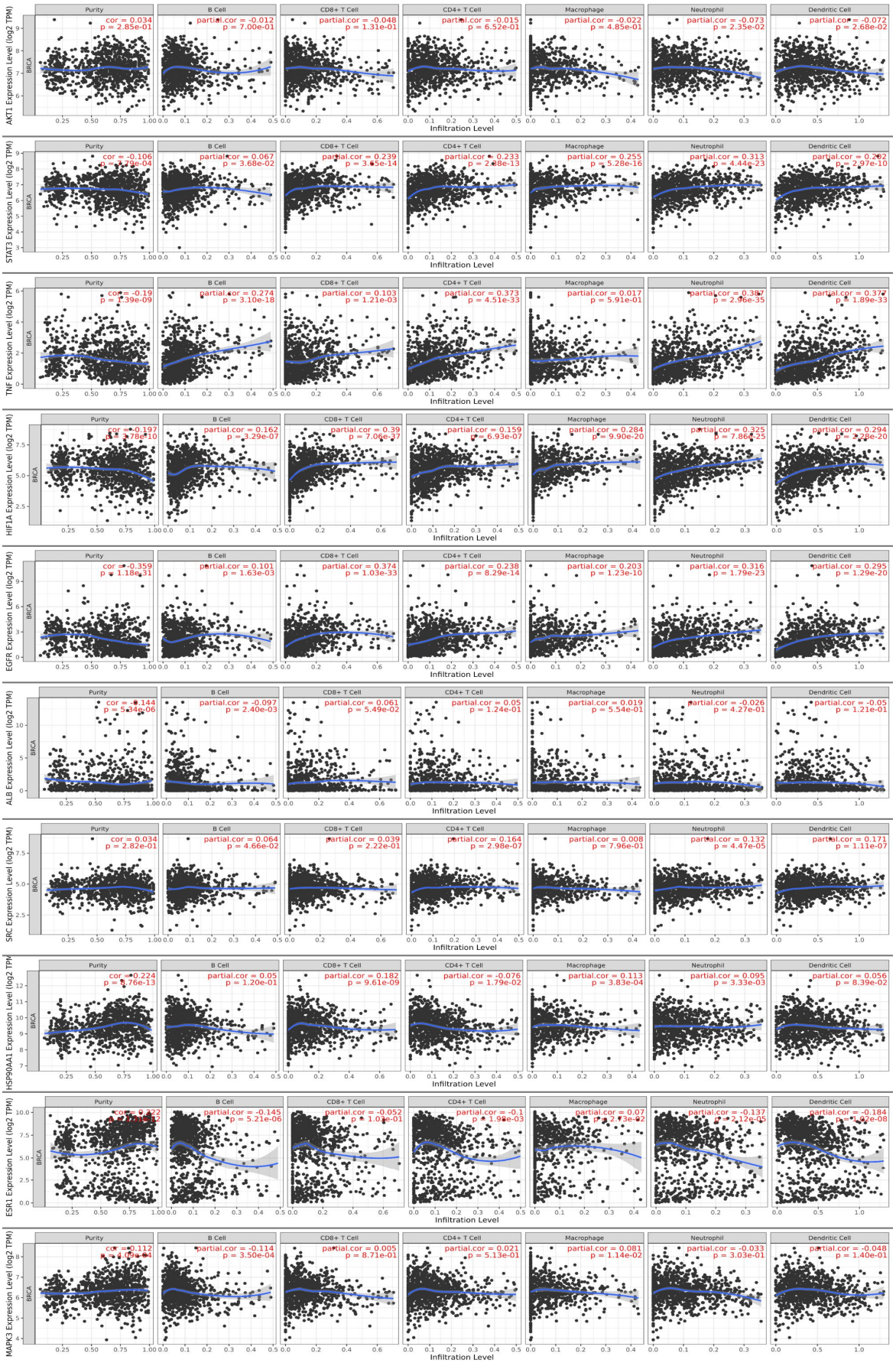

Figure 12. Correlation between hub gene expression and immune cell infiltration in breast invasive carcinoma (BRCA). The TIMER 2.0 database was used to correlate hub gene expression (AKT1, STAT3,

TNF, HIF1A, EGFR, ALB, SRC, HSP90AA1, ESR1, and MAPK3) with immune cell infiltration in TCGA Breast Invasive Carcinoma (BRCA) samples. Scatter graphs show the correlation between gene expression (log_2 TPM) and B cell, $CD8^+$ T cell, $CD4^+$ T cell, macrophage, neutrophil, and dendritic cell infiltration, as well as tumour purity. Each black dot represents a BRCA sample, while the blue line shows the fitted regression curve. Each panel shows partial Spearman's correlation coefficients (partial cor) adjusted for tumour purity and *p*-values in the upper-right corner. Positive correlation values imply that gene expression increases immune cell infiltration, while negative coefficients indicate the opposite. STAT3, TNF, and HIF1A had stronger positive correlations with multiple immune cell populations than AKT1, SRC, HSP90AA1, ESR1, and MAPK3, indicating that these hub genes modulate the breast cancer tumour immune microenvironment differently.

4. Discussion

Breast cancer remains one of the most prevalent malignancies among women worldwide, with triple-negative breast cancer (TNBC) representing a particularly aggressive and therapeutically challenging subtype. Defined by the absence of estrogen receptor (ER), progesterone receptor (PR), and HER2/ERBB2 expression, TNBC accounts for 10–15% of breast cancer cases and is characterized by high relapse rates, genomic heterogeneity, and poor prognosis. Standard treatments, such as anthracycline- or taxane-based chemotherapy, often result in rapid resistance and disease recurrence, underscoring the urgent need for more effective and less toxic therapeutic strategies.

A variety of plant-based natural extracts and compounds have been evaluated as candidate therapies for triple-negative breast cancer (TNBC). To date, more than 50 natural products and about 30 crude extracts have shown anti-TNBC activity by modulating a variety of signalling pathways. Most extracts are derived from terrestrial plants, while some originate from marine flora—*Pyracantha fortuneana*, dandelion, *Lippia origanoides*, *Dillenia suffruticosa*, *Cyperus rotundus*, *Calligonum comosum*, propolis, and *Benincasa hispida* seed are notable examples [31,32]. Representative natural compounds include dragmacidin D [33], sulforaphane [34], curcumenol [35], jatrophone [36], and galangin [18]. Recent comprehensive reviews further catalogue the expanding landscape of natural compounds under investigation for TNBC and their molecular targets [37–39], and integrated network-pharmacology/experimental-validation workflows analogous to the present study have recently been applied to other TNBC-directed natural compounds, e.g., nomilin [17].

In this study, the methanolic extract of *Alpinia officinarum* (AO) was evaluated for its therapeutic efficacy against triple-negative breast cancer (TNBC) using a combination of in vitro experiments and in silico analyses. Treatment with *Alpinia officinarum* (AO) produced significant cytotoxic effects in MDA-MB-231 cells, with an observed IC_{50} value of 31.1 μg/mL. At this concentration, AO primarily induced late-stage apoptosis, reflected by a substantial increase in the sub-G1 population. It also significantly reduced intracellular ROS levels and caused mitochondrial depolarization. Furthermore, AO modulated apoptotic signalling by affecting BCL-2 family proteins, particularly through the upregulation of the pro-apoptotic gene BAX.

It is worth noting that the observed decrease in steady-state intracellular ROS at 24 h post-treatment, measured alongside clear mitochondrial depolarisation and late-stage apoptosis, is not necessarily contradictory. The classic description of the mitochondrial (intrinsic) apoptotic pathway emphasises an early, often transient, burst of ROS that helps trigger mitochondrial permeability transition; however, because DCFH-DA fluorescence in the present study was captured at a single, comparatively late timepoint (24 h), it reflects the net steady-state redox status of the surviving cell population rather than the kinetics of ROS generation during the initiating phase of apoptosis. By 24 h, cells that have progressed into

late apoptosis typically show diminished mitochondrial electron-transport-chain activity and, consequently, a reduced capacity for further ROS production, which would present as an apparent net decrease in the population-level DCFH-DA signal even if an earlier ROS burst had already occurred and initiated the apoptotic cascade. In addition, *Alpinia officinarum* is rich in phenolic diarylheptanoids and flavonoids with well-documented direct free-radical-scavenging activity, and several classes of dietary polyphenols have been reported to induce mitochondria-dependent apoptosis through mechanisms that do not require a sustained rise in cytosolic ROS [40]. Taken together, these considerations offer a plausible biochemical explanation for the present findings; nonetheless, we agree that this observation warrants direct experimental clarification, and we recommend that future work include a kinetic, multi-timepoint assessment of ROS generation (e.g., at 1, 4, 12, and 24 h) alongside re-verification of the DCFH-DA staining protocol, to formally resolve the temporal relationship between the ROS response and the induction of apoptosis by AO.

The RT-PCR results additionally showed that BCL-2 and c-MYC transcript levels were largely unchanged, while BAD showed only a marginal decrease, in apparent contrast to the substantial increase in BAX. These findings are, however, consistent with well-established models of BCL-2-family regulation rather than contradictory to them. Induction of the intrinsic apoptotic pathway is governed less by the absolute expression of any single BCL-2-family member than by the relative BAX:BCL-2 ratio, which functions as a rheostat controlling mitochondrial outer-membrane permeabilisation; a marked rise in BAX alone, even without a corresponding fall in BCL-2, can be sufficient to shift this ratio toward apoptosis [41]. BAD's pro-apoptotic activity is regulated principally at the post-translational level: phosphorylation of BAD by AKT sequesters it in the cytoplasm bound to 14-3-3 proteins, whereas its dephosphorylation—rather than increased transcription—releases BAD to neutralise BCL-2/BCL-XL and promote apoptosis [42]. A modest change, or even a decrease, in BAD transcript level is therefore not inconsistent with an active pro-apoptotic role for BAD protein at the post-translational level, which was not assessed by RT-PCR in the present study. Notably, this places the RT-PCR findings in direct mechanistic continuity with the in silico hub-gene network: AKT1 and MAPK3 (ERK1)—two of the ten hub genes most strongly linked to the EGFR-TKI resistance pathway in our pathway-enrichment analysis—are the principal upstream kinases controlling BAD phosphorylation and BAX activation, respectively. This suggests that AO's cytotoxic action in MDA-MB-231 cells may converge on the same AKT1/MAPK3–BAD/BAX signalling axis nominated by the network pharmacology analysis, providing a coherent link between the computationally predicted hub genes and the empirically observed apoptotic gene-expression changes. The absence of a corresponding decrease in c-MYC transcript at 24 h may indicate that, at this early timepoint and dose, AO principally engages the mitochondrial apoptotic machinery rather than directly suppressing MYC-driven proliferative transcription; whether prolonged exposure or higher concentrations modulate c-MYC expression remains to be tested.

These findings were further supported by in silico analysis. Computational screening identified 199 genes commonly associated with *Alpinia officinarum* (AO) and triple-negative breast cancer (TNBC). These genes were involved in several key pathways, including the EGFR tyrosine kinase inhibitor (TKI) resistance, PI3K-Akt, apoptosis, proteoglycans in cancer, microRNAs in cancer, and MAPK signalling pathways. Ten hub genes were identified—AKT1, STAT3, TNF, HIF1A, EGFR, ALB, SRC, HSP90AA1, ESR1, and MAPK3—which were consistently linked to the top enriched pathways. Among these, the EGFR-TKI resistance pathway appears to play a central role in AO's mechanism of action, influencing important cancer-related processes like cell growth, survival, proliferation, and

angiogenesis. Additionally, in breast cancer tissue samples, increased mRNA expression of AKT1, ESR1, and SRC was observed.

Analysis of immune infiltration showed that STAT3, TNF and HIF1A were the key mediators between the tumour immune microenvironment and oncogenic signalling in breast cancer. The positive correlations with innate (macrophages, neutrophils, and dendritic cells) and adaptive immune cell populations ($CD4^+$ and $CD8^+$ T cells) emphasise their role in the modulation of inflammatory responses and establishment of antitumor immunity. In contrast, AKT1, SRC and HSP90AA1 appear to mainly act via cell-autonomous mechanisms impacting migration, proliferation, survival and protein homeostasis, with little effect on immune cell recruitment. The negative link between ESR1 expression and immune infiltration further supports the widely documented dichotomy of more immunogenic breast cancer subtypes against luminal, oestrogen receptor positive tumours which are generally marked by lower immune infiltration. All these results indicate the crosstalk between oncogenic pathways and the immune system, and may help to identify biomarkers of immunotherapeutic stratification in breast cancer.

To date, no studies have evaluated AO in the context of TNBC, and its mechanism of action remains unexplored through in silico approaches. Existing in vitro research has been limited to luminal-type breast cancer models like the MCF-7 cell line (ER^+, PR^+, $HER2^+$), rather than the triple-negative MDA-MB-231 cell line (ER^-, PR^-, $HER2^-$), which represents TNBC.

Previous work has shown that a methanolic extract of AO triggers apoptosis in MCF-7 cells through caspase activation and mitochondrial disruption, accompanied by S-phase arrest and down-regulation of the S-phase regulators CDK2, cyclin A, and E2F1 [43]. Diarylheptanoid constituents of AO—such as α,β-unsaturated ketones—have likewise exhibited cytotoxicity in MCF-7 cells, increasing the sub-G1 fraction and inducing ROS-dependent mitochondrial and lysosomal dysfunction, thereby promoting apoptosis [44].

Our research identified *Alpinia officinarum* (AO) as a promising multi-targeted candidate against TNBC, supported by both in vitro cytotoxicity and in silico pathway analysis. However, to translate these preliminary results into clinical relevance, further in vivo investigations are essential. These studies should assess AO's therapeutic efficacy, toxicity, and mechanistic pathways in animal models, paving the way for future clinical applications.

Nonetheless, this study has several limitations that temper the strength of these conclusions and define clear next steps: the specific extract used has not yet been chemically fingerprinted against its plant material or region of origin, and all findings derive from a single TNBC cell line in vitro. Addressing these limitations together with in vivo efficacy and toxicity studies will be essential before AO can be considered a credible candidate for multi-targeted TNBC drug development.

5. Conclusions

Our research concluded that the methanolic extract of *Alpinia officinarum* (AO) demonstrated notable cytotoxicity against TNBC cells in vitro, inducing apoptosis, mitochondrial dysfunction, and cell cycle arrest. These findings were complemented by in silico analyses, which identified key molecular targets and pathways, most notably the EGFR-TKI resistance pathway, potentially underlying AO's therapeutic effects. Our findings, therefore, underscore AO's potential as a multi-targeted candidate for TNBC therapy and provide a strong basis for further in vivo validation. More specifically, AO exhibited an IC50 of 31.1 ± 4.5 μg/mL against MDA-MB-231 cells—comparable to the reference drug carboplatin (IC50 31.6 ± 8.1 μg/mL)—and drove a pronounced increase in late-apoptotic cells (23.5% vs. 1.96% in controls), mitochondrial depolarisation ($\Delta\Psi m$ MFI 360 vs. 3071 in controls), and BAX upregulation, while also inhibiting MDA-MB-231 migration. In parallel,

network pharmacology analysis exhibited ten hub genes (AKT1, STAT3, TNF, HIF1A, EGFR, ALB, SRC, HSP90AA1, ESR1, and MAPK3), converging on the EGFR-TKI resistance, PI3K-AKT, and MAPK signalling pathways, with UALCAN and TIMER2.0 analyses further indicating elevated expression of several hub genes (AKT1, ESR1, SRC) in breast cancer tissue and distinct immune-infiltration profiles for inflammation-associated genes (STAT3, TNF, HIF1A) versus cell-autonomous signalling genes (AKT1, SRC, HSP90AA1). Together, the convergence of the AKT1/MAPK3-centred hub-gene network with the empirically observed BAX-dominant, BAD/BCL-2/c-MYC-sparing apoptotic gene-expression signature strengthens the mechanistic plausibility of AO's anti-TNBC activity.

Supplementary Materials: The following supporting information can be downloaded at: https://www.mdpi.com/article/10.3390/joma3020021/s1.

Author Contributions: S.S. provided methodology, data curation, software and formal analysis, and writing the original draft. P.S. helped with data curation, formal analysis, software, and methodology. A.D.J. supervised and helped review and edit. V.S.L. conceived the study and performed formal analysis, investigation, validation, and helped write the original daft. All authors have read and agreed to the published version of the manuscript.

Funding: This research received no external funding.

Institutional Review Board Statement: Not applicable.

Informed Consent Statement: Not applicable.

Data Availability Statement: The datasets used and/or analyzed during the current study are available from the corresponding author on reasonable request.

Acknowledgments: The authors gratefully acknowledge Rojatkar for providing the *Alpinia officinarum* (AO) extract used in this study and for generously sharing detailed information regarding its preparation.

Conflicts of Interest: Author Amol Dilip Jadhav was employed by the company Nirav BioSolutions Pvt Ltd. The remaining authors declare that the research was conducted in the absence of any commercial or financial relationships that could be construed as a potential conflict of interest.

Abbreviations

The following abbreviations are used in this manuscript:

AO	*Alpinia officinarum*
BA	Bioactive compounds
BAX	BCL-2 associated X gene
BCL2	B-cell lymphoma 2
DAVID	Database for Annotation, Visualization and Integrated Discovery
DisGeNET	Disease Gene Networks
EGFR	Epidermal Growth Factor Receptor
ER	Estrogen receptor
GO	Gene ontology
HER2	Human Epidermal Growth Factor Receptor 2
IC50	Inhibitory Concentration
KEGG	Kyoto Encyclopedia of Genes and Genomes
MCF-7	Michigan Cancer Foundation-7
MDA-MB-231	M D Anderson Metastatic Breast 231
MMP	Mitochondrial Membrane Potential
PI3K-AKT	Phosphoinositide 3-kinase–Protein Kinase B
PPI	Protein–protein interaction
PR	Progesterone receptor

ROS	Reactive oxygen species
RT-PCR	Real time Polymerase Chain Reaction
STRING	Search Tool for the Retrieval of Interacting Genes
TIMER	Tumor Immune Estimation Resource
TKI	Tyrosine Kinase Inhibitor
TNBC	Triple-negative Breast Cancer
UALCAN	University of ALabama at Birmingham CANcer data analysis Portal
ANOVA	Analysis of Variance
CCCP	Carbonyl cyanide m-chlorophenylhydrazone
DCFH-DA	2′,7′-Dichlorodihydrofluorescein diacetate
DMSO	Dimethyl sulfoxide
FBS	Fetal Bovine Serum
FDA	U.S. Food and Drug Administration
IMPPAT	Indian Medicinal Plants, Phytochemistry and Therapeutics (database)
MFI	Mean Fluorescence Intensity
MTT	3-(4,5-Dimethylthiazol-2-yl)-2,5-diphenyltetrazolium bromide
PBS	Phosphate-Buffered Saline
SD	Standard Deviation
SMILES	Simplified Molecular Input Line Entry System
TCGA	The Cancer Genome Atlas

References

1. Brown, J.S.; Amend, S.R.; Austin, R.H.; Gatenby, R.A.; Hammarlund, E.U.; Pienta, K.J. Updating the Definition of Cancer. *Mol. Cancer Res.* **2023**, *21*, 1142–1147. [CrossRef]
2. Roy, P.S.; Saikia, B.J. Cancer and cure: A critical analysis. *Indian J. Cancer* **2016**, *53*, 441–442. [CrossRef]
3. Wendlocha, D.; Krzykawski, K.; Mielczarek-Palacz, A.; Kubina, R. Selected Flavonols in Breast and Gynecological Cancer: A Systematic Review. *Nutrients* **2023**, *15*, 2938. [CrossRef]
4. Cragg, G.M.; Pezzuto, J.M. Natural Products as a Vital Source for the Discovery of Cancer Chemotherapeutic and Chemopreventive Agents. *Med. Princ. Pract.* **2016**, *25*, 41–59. [CrossRef]
5. Arnold, M.; Morgan, E.; Rumgay, H.; Mafra, A.; Singh, D.; Laversanne, M.; Vignat, J.; Gralow, J.R.; Cardoso, F.; Siesling, S.; et al. Current and future burden of breast cancer: Global statistics for 2020 and 2040. *Breast* **2022**, *66*, 15–23. [CrossRef]
6. Torre, L.A.; Siegel, R.L.; Ward, E.M.; Jemal, A. Global cancer incidence and mortality rates and trends—An update. *Cancer Epidemiol. Biomark. Prev.* **2016**, *25*, 16–27. [CrossRef]
7. Trayes, K.P.; Cokenakes, S.E.H. Breast Cancer Treatment. *Am. Fam. Physician* **2021**, *104*, 171–178.
8. Dass, S.A.; Tan, K.L.; Rajan, R.S.; Mokhtar, N.F.; Adzmi, E.R.M.; Rahman, W.F.W.A.; Din, T.A.D.A.-A.T.; Balakrishnan, V. Triple Negative Breast Cancer: A Review of Present and Future Diagnostic Modalities. *Medicina* **2021**, *57*, 62. [CrossRef]
9. McDonald, E.S.; Clark, A.S.; Tchou, J.; Zhang, P.; Freedman, G.M. Clinical diagnosis and management of breast cancer. *J. Nucl. Med.* **2016**, *57*, 9S–16S. [CrossRef]
10. Shien, T.; Iwata, H. Adjuvant and neoadjuvant therapy for breast cancer. *Jpn. J. Clin. Oncol.* **2020**, *50*, 225–229. [CrossRef]
11. Obidiro, O.; Battogtokh, G.; Akala, E.O. Triple Negative Breast Cancer Treatment Options and Limitations: Future Outlook. *Pharmaceutics* **2023**, *15*, 1796. [CrossRef]
12. Yuan, Y.; Long, H.; Zhou, Z.; Fu, Y.; Jiang, B. PI3K–AKT-Targeting Breast Cancer Treatments: Natural Products and Synthetic Compounds. *Biomolecules* **2023**, *13*, 93. [CrossRef]
13. Lei, X.; Wang, J.; Zuo, K.; Xia, T.; Zhang, J.; Xu, X.; Liu, Q.; Li, X. *Alpinia officinarum* Hance: A comprehensive review of traditional uses, phytochemistry, pharmacokinetic and pharmacology. *Front. Pharmacol.* **2024**, *15*, 1414635. [CrossRef]
14. Abubakar, I.B.; Malami, I.; Yahaya, Y.; Sule, S.M. A review on the ethnomedicinal uses, phytochemistry and pharmacology of *Alpinia officinarum* Hance. *J. Ethnopharmacol.* **2018**, *224*, 45–62. [CrossRef]
15. Azmi, A.S. Adopting Network Pharmacology for Cancer Drug Discovery. *Curr. Drug Discov. Technol.* **2013**, *10*, 95–105. [CrossRef]
16. Tang, J.; Aittokallio, T. Network Pharmacology Strategies Toward Multi-Target Anticancer Therapies: From Computational Models to Experimental Design Principles. *Curr. Pharm. Des.* **2014**, *20*, 23–36. [CrossRef]
17. Wu, Z.; Xiang, H.; Wang, X.; Zhang, R.; Guo, Y.; Qu, L.; Zhou, J.; Xiao, Y. Integrating network pharmacology, molecular docking and experimental verification to explore the therapeutic effect and potential mechanism of nomilin against triple-negative breast cancer. *Mol. Med.* **2024**, *30*, 166. [CrossRef]

18. Sinnarkar, S.; Suryawanshi, P.; Dilip, A.; Bhawalkar, J.; Ladke, V. Galangin promotes apoptosis by upregulating the pro-apoptotic gene BAX in triple-negative breast cancer. *J. Egypt. Natl. Cancer Inst.* **2024**, *36*, 41. [CrossRef]
19. Brandt, R.; Keston, A.S. Synthesis of diacetyldichlorofluorescin: A stable reagent for fluorometric analysis. *Anal. Biochem.* **1965**, *11*, 6–9. [CrossRef]
20. Liang, C.C.; Park, A.Y.; Guan, J.L. In vitro scratch assay: A convenient and inexpensive method for analysis of cell migration in vitro. *Nat. Protoc.* **2007**, *2*, 329–333. [CrossRef]
21. Daina, A.; Michielin, O.; Zoete, V. SwissADME: A free web tool to evaluate pharmacokinetics, drug-likeness and medicinal chemistry friendliness of small molecules. *Sci. Rep.* **2017**, *7*, 42717. [CrossRef]
22. Daina, A.; Michielin, O.; Zoete, V. SwissTargetPrediction: Updated data and new features for efficient prediction of protein targets of small molecules. *Nucleic Acids Res.* **2019**, *47*, W357–W364. [CrossRef]
23. Lin, J.S.; Lai, E.M. Protein–Protein Interactions: Co-Immunoprecipitation. In *Methods in Molecular Biology*; Humana Press: New York, NY, USA, 2017; Volume 1615, pp. 211–219. [CrossRef]
24. Shannon, P.; Markiel, A.; Ozier, O.; Baliga, N.S.; Wang, J.T.; Ramage, D.; Amin, N.; Schwikowski, B.; Ideker, T. Cytoscape: A Software Environment for Integrated Models of Biomolecular Interaction Networks. *Genome Res.* **2003**, *13*, 2498–2504. [CrossRef]
25. Kanehisa, M.; Furumichi, M.; Sato, Y.; Ishiguro-Watanabe, M.; Tanabe, M. KEGG: Integrating viruses and cellular organisms. *Nucleic Acids Res.* **2021**, *49*, D545–D551. [CrossRef]
26. Ashburner, M.; Ball, C.A.; Blake, J.A.; Botstein, D.; Butler, H.; Cherry, J.M.; Davis, A.P.; Dolinski, K.; Dwight, S.S.; Eppig, J.T.; et al. Gene ontology: Tool for the unification of biology. *Nat. Genet.* **2000**, *25*, 25–29. [CrossRef]
27. Ge, S.X.; Jung, D.; Jung, D.; Yao, R. ShinyGO: A graphical gene-set enrichment tool for animals and plants. *Bioinformatics* **2020**, *36*, 2628–2629. [CrossRef]
28. Chandrashekar, D.S.; Karthikeyan, S.K.; Korla, P.K.; Patel, H.; Shovon, A.R.; Athar, M.; Netto, G.J.; Qin, Z.S.; Kumar, S.; Manne, U.; et al. UALCAN: An update to the integrated cancer data analysis platform. *Neoplasia* **2022**, *25*, 18–27. [CrossRef]
29. Huang, L.; Fu, L. Mechanisms of resistance to EGFR tyrosine kinase inhibitors. *Acta Pharm. Sin. B* **2015**, *5*, 390–401. [CrossRef]
30. Luo, W.; Brouwer, C. Pathview: An R/Bioconductor package for pathway-based data integration and visualization. *Bioinformatics* **2013**, *29*, 1830–1831. [CrossRef]
31. Chen, H.; Yang, J.; Yang, Y.; Zhang, J.; Xu, Y.; Lu, X. The Natural Products and Extracts: Anti-Triple-Negative Breast Cancer In Vitro. *Chem. Biodivers.* **2021**, *18*, e2001047. [CrossRef]
32. Kanase, M.; Dharkar, N.; Ladke, V.S. Evaluating the Efficacy of Benincasa Hispida Seed Extract in Inhibiting the Proliferation of a Human Triple Negative Breast Cancer Cell Line. *Asian Pac. J. Cancer Prev.* **2025**, *26*, 471–478. [CrossRef]
33. Guzmán, E.A.; Peterson, T.A.; Wright, A.E. The Marine Natural Compound Dragmacidin D Selectively Induces Apoptosis in Triple-Negative Breast Cancer Spheroids. *Mar. Drugs* **2023**, *21*, 642. [CrossRef]
34. Zhang, Y.; Lu, Q.; Li, N.; Xu, M.; Miyamoto, T.; Liu, J. Sulforaphane suppresses metastasis of triple-negative breast cancer cells by targeting the RAF/MEK/ERK pathway. *npj Breast Cancer* **2022**, *8*, 40. [CrossRef]
35. Li, F.; Qi, Q.; Qiao, Y.; Huang, Y.; Lu, Y.; Gu, K.; Liu, H.; Gao, C.; Liu, S.; Wu, H. Curcumenol inhibits malignant progression and promotes ferroptosis via the SLC7A11/NF-κB/TGF-β pathway in triple-negative breast cancer. *Int. J. Mol. Med.* **2025**, *56*, 111. [CrossRef]
36. Fatima, I.; El-Ayachi, I.; Taotao, L.; Lillo, M.A.; Krutilina, R.I.; Seagroves, T.N.; Radaszkiewicz, T.W.; Hutnan, M.; Bryja, V.; Krum, S.A.; et al. The natural compound Jatrophone interferes with Wnt/β-catenin signaling and inhibits proliferation and EMT in human triple-negative breast cancer. *PLoS ONE* **2017**, *12*, e0197796. [CrossRef]
37. Jiménez-Flores, E.; Reytor-González, C.; Jima Gavilanes, C.; Carrillo, C.; Horowitz, R.; Cárdenas Carrera, J.C.; Bigoni-Ordóñez, G.D.; Simancas-Racines, D. Bioactive Natural Compounds in Triple-Negative Breast Cancer: Molecular Targets and Therapeutic Perspectives. *Pharmaceuticals* **2026**, *19*, 550. [CrossRef]
38. Li, Q.; Ye, Z.; Wang, G.; Chen, Y.; Deng, J.; Wang, D.; Wang, Y. Natural Products as Novel Therapeutic Agents for Triple-Negative Breast Cancer: Current Evidence, Mechanisms, Challenges, and Opportunities. *Molecules* **2025**, *30*, 1201. [CrossRef]
39. Kaleem, M.; Thool, M.; Dumore, N.G.; Abdulrahman, A.O.; Ahmad, W.; Almostadi, A.; Alhashmi, M.H.; Kamal, M.A.; Tabrez, S. Management of triple-negative breast cancer by natural compounds through different mechanistic pathways. *Front. Genet.* **2024**, *15*, 1440430. [CrossRef]
40. Vidjeyamannane, C.; Joy, A.; Prakash, K.; Saravanakumar, R. A comprehensive review on the role of plant-derived bioactive metabolites driving ROS-mediated apoptosis in cancer. *Med. Oncol.* **2025**, *42*, 420. [CrossRef]
41. Oltvai, Z.N.; Milliman, C.L.; Korsmeyer, S.J. Bcl-2 heterodimerizes in vivo with a conserved homolog, Bax, that accelerates programmed cell death. *Cell* **1993**, *74*, 609–619. [CrossRef]
42. Datta, S.R.; Dudek, H.; Tao, X.; Masters, S.; Fu, H.; Gotoh, Y.; Greenberg, M.E. Akt phosphorylation of BAD couples survival signals to the cell-intrinsic death machinery. *Cell* **1997**, *91*, 231–241. [CrossRef]

43. Ghil, S. Antiproliferative activity of *Alpinia officinarum* extract in the human breast cancer cell line MCF-7. *Mol. Med. Rep.* **2013**, *7*, 1288–1292. [CrossRef]
44. Gamre, S.; Tyagi, M.; Chatterjee, S.; Patro, B.S.; Chattopadhyay, S.; Goswami, D. Synthesis of Bioactive Diarylheptanoids from *Alpinia officinarum* and Their Mechanism of Action for Anticancer Properties in Breast Cancer Cells. *J. Nat. Prod.* **2021**, *84*, 352–363. [CrossRef]

Disclaimer/Publisher's Note: The statements, opinions and data contained in all publications are solely those of the individual author(s) and contributor(s) and not of MDPI and/or the editor(s). MDPI and/or the editor(s) disclaim responsibility for any injury to people or property resulting from any ideas, methods, instructions or products referred to in the content.